Reflection of Noble Gas Ions at Solid Surfaces

HOMER D. HAGSTRUM
Bell Telephone Laboratories, Murray Hill, New Jersey
(Received March 22, 1961)

A method has been developed for distinguishing the reflection of ions at solid surfaces as ions or as metastable atoms. Results are given for He^+, Ne^+, and Ar^+ ions incident on clean W, Mo, and Si(100) and on contaminated W, Hf, and Ge(111) surfaces. The reflection coefficient of ions to ions (R_{ii}) is found to be small (0.0004 to 0.002) and essentially independent of incident ion energy. The reflection coefficient of ions to metastable atoms (R_{im}) is found to increase with ion energy from values comparable to R_{ii} at 10 ev to values as high as 0.04 at 1000 ev. Discussion of these results is given in terms of the known resonance and Auger transitions which can occur near a solid surface for ions of sufficiently large ionization energy. It is shown that the results can be accounted for only if ions are transformed to metastable atoms very close to the surface, and a possible mechanism for this process is proposed.

I. INTRODUCTION

THE present work deals with the reflection of ions of large ionization energy at the surfaces of solids. Very little work has been done in this field to date and the phenomena are complex and not well understood. Oliphant[1] observed that positive ions could be reflected as metastable atoms, particularly at grazing incidence. Healea and co-workers[2,3] found that H^+, He^+, Ne^+, and Ar^+ were reflected in appreciable amounts from a nickel surface and Rostagni[4] observed reflection of noble gas ions at a copper surface. Other observations of relevance are those concerning the reflection of metastable atoms[1,5] and the formation of negative ions from positive ions at surfaces.[6] More recently, Honig[7] and Bradley and his co-workers[8–10] have mass analyzed the ionic products released from metal surfaces under the impact of noble gas ions. A comparison of the present results with this previous work is made in Sec. IV.

Much more work has been done on the reflection of ions of low ionization energy such as the alkalis. A recent review and evaluation of this work is to be found in the article by Brunnée[11] and a theoretical treatment has been given by von Roos.[12] Brunnée has suggested that alkali ion reflection should be considerably larger and hence easier to study than the reflection of ions of large ionization energy because of the high neutralization rate of the latter at the surface. This neutralization occurs for clean and lightly contaminated surfaces by virtue of the Auger-type electronic transitions possible for these ions.

In the present investigation an attempt has been made to work with demonstrably clean, as well as contaminated, surfaces and to distinguish experimentally between reflected ions and metastable atoms. The data have been collected over a number of years in connection with the experimental studies of electron ejection in the Auger-type neutralization of noble gas ions at solid surfaces.[13–17] Some sketchy preliminary reports of the findings on ion reflection are to be found in these papers and others.[18,19]

II. EXPERIMENT

The present experimental results were obtained with the apparatus described elsewhere.[18] A beam of noble gas ions is produced by electron impact, focused, stopped down, and in some cases mass analyzed. Eventually, this focused beam of controllable kinetic energy enters a spherical electron collector, S, and strikes the surface of the target, T, situated at the center of the sphere as indicated in Fig. 1. Primary ion beam currents are of the order of 10^{-10} amp in this work. With no voltage, V_{ST}, between sphere and target the primary, secondary, and tertiary currents indicated in Fig. 1(a) and Table I flow. Here the symbol I is used to indicate the magnitude of a space current of particles whose nature is specified by the superscript, i for ions, e for electrons, and m for metastable atoms. The subscripts indicate the currents to which the current in question is secondary (single subscript, or second subscript if there are two) and tertiary (first subscript of two), as the case may be. If the particle is charged, the same symbol is used to designate the electric current carried by the particles. I_S and I_T are the electric currents measured at electrodes S and T

[1] M. L. E. Oliphant, Proc. Roy. Soc. (London) **A124**, 228 (1929).
[2] M. Healea and E. L. Chaffee, Phys. Rev. **49**, 925 (1936).
[3] M. Healea and C. Houtermans, Phys. Rev. **58**, 608 (1940).
[4] A. Rostagni, Ricerca sci. **9**, 633 (1938).
[5] D. Greene, Proc. Phys. Soc. (London) **B63**, 876 (1950).
[6] Reviews of this work are to be found in Sec. 4 of Chap. 9 of H. S. W. Massey and E. H. S. Burhop, *Electronic and Ionic Impact Phenomena* (Clarendon Press, Oxford, 1952), and in L. B. Loeb, *Handbuch der Physik*, edited by S. Flügge (Springer-Verlag, Berlin, 1956), Vol. 21, p. 445.
[7] R. E. Honig, J. Appl. Phys. **29**, 549 (1958).
[8] R. C. Bradley, J. Appl. Phys. **30**, 1 (1959).
[9] R. C. Bradley, A. Arking, and D. S. Beers, J. Chem. Phys. **33**, 764 (1960).
[10] R. C. Bradley and E. Ruedl, Bull. Am. Phys. Soc. **5**, 16 (1960).
[11] C. Brunnée, Z. Physik **147**, 161 (1957).
[12] O. von Roos, Z. Physik **147**, 184 (1957).
[13] H. D. Hagstrum, Phys. Rev. **89**, 244 (1953); **104**, 672 (1956).
[14] H. D. Hagstrum, Phys. Rev. **91**, 543 (1953).
[15] H. D. Hagstrum, Phys. Rev. **96**, 325 (1954).
[16] H. D. Hagstrum, Phys. Rev. **119**, 940 (1960).
[17] H. D. Hagstrum, J. Appl. Phys. **28**, 323 (1957).
[18] H. D. Hagstrum, Rev. Sci. Instr. **24**, 1122 (1953), Sec. IX.
[19] H. D. Hagstrum, Phys. Rev. **93**, 652 (1954).

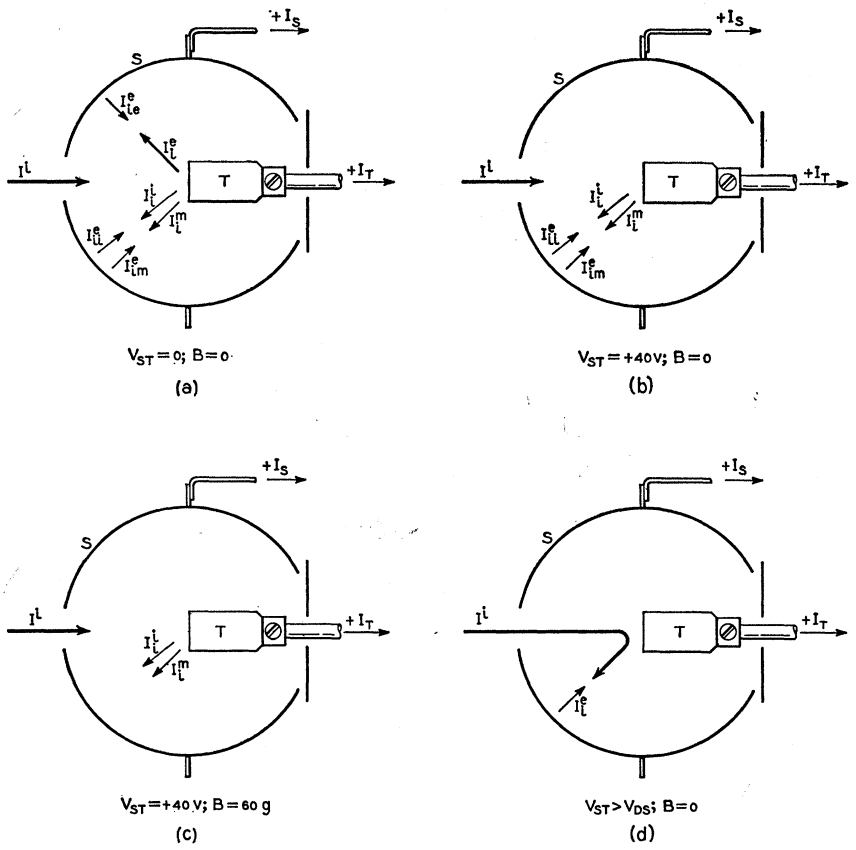

FIG. 1. Schematic indication of the primary, secondary, and tertiary currents which flow between target and spherical electron collector in four situations used in the present work. Notation is defined in Table I.

whose positive directions are indicated by the arrows alongside the symbols in Fig. 1.

The particle currents flowing under conditions of Fig. 1(a) are the primary ion beam I^i, the Auger electrons ejected from the sphere by these ions, $I_i{}^e$, the reflected ions, $I_i{}^i$, the reflected metastable atoms, $I_i{}^m$, and, finally, the electrons ejected from the inside of the sphere by each of the particle currents emanating from the target. Currents of higher order than those specified may safely be neglected for reasons given below.

As V_{ST} is increased positively from zero (T positive with respect to S), the Auger electron current $I_i{}^e$ is retarded to zero. This produces the $\rho=I_S/(I_T+I_S)$ vs V_{ST} characteristic which has been analyzed in Sec. IX of reference 18. It suffices to know here that for V_{ST} greater than the maximum kinetic energy of the electrons comprising $I_i{}^e$, $I_i{}^e$ and $I_{ie}{}^e$ are zero. Under these conditions the remaining secondary and tertiary currents are accelerated to the opposite electrode [Fig. 1(b)]. The reverse would be the case for ions reflected at the sphere. Such a higher order ion current could thus only with difficulty reach the target where, if it did, any electrons ejected by it would be held by the electric field. It is for this reason that higher order currents than those shown in Fig. 1 are neglected.

Under the conditions of Fig. 1(b) the currents to target and sphere are

$$I_T=I^i-I_i{}^i-I_{ii}{}^e-I_{im}{}^e, \quad (1)$$

$$I_S=I_i{}^i+I_{ii}{}^e+I_{im}{}^e. \quad (2)$$

The quantity $\rho=I_S/(I_T+I_S)$ under the conditions of

TABLE I. Definitions of notation.

I^i	primary ion bean
$I_i{}^e$	Auger electrons ejected by I^i
$I_{ie}{}^e$	electrons ejected by $I_i{}^e$ at sphere
$I_i{}^i$	ions produced by reflection of I^i
$I_{ii}{}^e$	electrons ejected by $I_i{}^i$ at sphere
$I_i{}^m$	metastable atoms produced by reflection of I^i
$I_{im}{}^e$	electrons ejected by $I_i{}^m$ at sphere
I_S	current to sphere
I_T	current to target
R_{ii}	reflection coefficient of ions to ions, $I_i{}^i/I^i$
R_{im}	reflection coefficient of ions to metastable atoms, $I_i{}^m/I^i$
R_0	$\rho=I_S/(I_T+I_S)$ with no B field
R_B	$\rho=I_S/(I_T+I_S)$ with B field
γ_i	electron yield at target per incident ion, $I_i{}^e/I^i$
γ_i'	electron yield at sphere per incident ion, $I_{ii}{}^e/I_i{}^i$
γ_m'	electron yield at sphere per incident metastable atom, $I_{im}{}^e/I_i{}^m$

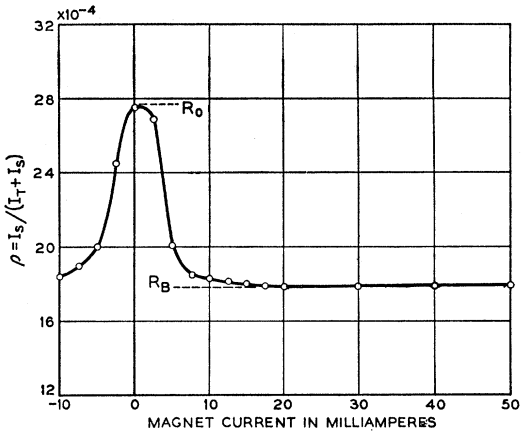

FIG. 2. Plot of $\rho = I_S/(I_T+I_S)$ against magnet current, showing the suppression of electronic currents in going from R_0 [part (b) of Fig. 1] to R_B [part (c) of Fig. 1]. The magnetic field produced at the target surface is 2.4 gauss per ma.

Fig. 1(b) is called R_0 and may be written

$$R_0 = \left(\frac{I_S}{I_T+I_S}\right)_{B=0} = \frac{I_i^i + I_{ii}^e + I_{im}^e}{I^i}. \tag{3}$$

Using the reflection coefficients and electron yield parameters defined in Table I, (3) becomes:

$$R_0 = R_{ii} + \gamma_i' R_{ii} + \gamma_m' R_{im}. \tag{4}$$

The quantity R_0 is thus a mixture of effects caused by reflected ions and reflected metastable atoms. It is the quantity measured after the Auger electron current has been retarded out. It should not be confused with R_{ii} which it includes (see Sec. IV). In order to separate R_0 into its component parts a magnetic field is applied in the target region perpendicular to the plane of Fig. 1. A field of 60 gauss is sufficient to suppress essentially completely all of the electronic currents flowing in part (b) of Fig. 1, leaving only the particle currents shown in part (c). The quantity ρ is now

$$R_B = \left(\frac{I_S}{I_T+I_S}\right)_{B=B} = \frac{I_i^i}{I^i} = R_{ii}. \tag{5}$$

Thus with the magnetic field on we measure directly the reflection coefficient of ions to ions, one of the three unknowns in Eq. (4).

A second unknown in Eq. (4), namely γ_i', the electron yield for ions incident on the inside of the sphere, may be measured under the conditions shown in Fig. 1(d). Here, with $B=0$, the voltages of sphere S and target T are arranged relative to the source of ions at electrode D such that the entire ion beam is repelled by the target and strikes the sphere. The roles of sphere and target current are now reversed and

$$\gamma_i' = \left(\frac{I_T}{I_S+I_T}\right)_{V_{ST}>V_{DS}}. \tag{6}$$

(Further details concerning this type of measurement may be obtained from Fig. 10 and accompanying discussion in reference 18.)

The third unknown in Eq. (4), the electron yield for metastable atoms incident on the sphere, γ_m', cannot be measured. However, there are good reasons to believe that the yields for ions and metastable atoms are equal,[20,21] that is, that

$$\gamma_m' = \gamma_i'. \tag{7}$$

Now we know all the parameters in Eq. (4) which we may solve for R_{im} using Eq. (5). Thus we obtain the following expressions for R_{ii} and R_{im} in terms of the experimental quantities R_0 and R_B:

$$R_{ii} = R_B, \tag{8}$$

$$R_{im} = [R_0 - (1+\gamma_i')R_B]/\gamma_i'. \tag{9}$$

The experiment consists of measuring the currents I_S and I_T under the sets of conditions given in parts (b)–(d) of Fig. 1. From these data R_0, R_B, and γ_i' may be calculated by Eqs. (3), (5), and (6) and R_{ii} and R_{im} by Eqs. (8) and (9) assuming (7). There remains only to discuss the effectiveness of the magnetic field in suppressing the electronic currents I_{ii}^e and I_{im}^e.

In Fig. 2, ρ is plotted as a function of magnet current. We note that ρ is maximum as expected for zero field and saturates well above 20 ma. Only those electrons with velocity vectors inside two opposing cones coaxial with the magnetic field may reach the target. The included angle of these cones decreases as the magnetic field increases. The excellent saturation of the characteristic in Fig. 2 is taken as evidence of the effectiveness

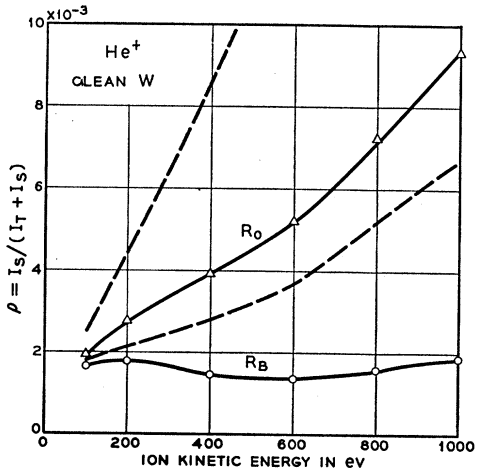

FIG. 3. Plots of R_0 and R_B for He^+ ions incident on clean W. The dashed curves indicate limits on the R_0 curve observed for various conditions of the surface of the sphere affecting the quantity γ_i'. R_B is unaffected by these changes in R_0 as is explained in the text.

[20] H. D. Hagstrum, Phys. Rev. **96**, 336 (1954).
[21] H. D. Hagstrum, J. Appl. Phys. **31**, 897 (1960).

of the field in suppressing the electronic currents. Data were generally taken at a magnet current of 25 ma corresponding to a field of 60 gauss.

III. RESULTS

Measurements of R_0 and R_B as functions of incident ion energy for He^+ ions on clean tungsten are shown in Fig. 3. These may be taken as typical of the R_0, R_B data obtained in this work. When the γ_i' at the sphere was changed by heating the sphere or by adsorbing gas on it, R_0 curves in the range indicated between the dashed lines in Fig. 3 were obtained *without* changing the R_B curve. This is consistent with the fact that R_B depends only on R_{ii} [Eq. (5)] and hence is independent of conditions at the sphere. R_0, on the other hand, does depend upon electron yields at the sphere [Eq. (4)].

Measurements of γ_i' are shown in Fig. 4. Curves 1, 2, and 3 are for He^+, Ne^+, Ar^+ ions, respectively. These data were taken during the tungsten experiment when the sphere used was made of tantalum. The sphere surface was certainly not clean, as is evidenced by the changes which could be made in γ_i' indicated above. Curve 4 is the yield measured for a Ta target in the work of reference 14. The data of Fig. 4 were used in reducing the data for W, Mo, and Hf in Tables II and III. γ_i' was not measured in the work with Si and Ge in which the sphere was made of Nichrome V. However, it has been found that contaminated metals show Auger yields which do not differ greatly from one another. Consequently, the data of Fig. 4 were used in reducing the Si and Ge data also. Any error introduced in this way would affect only the magnitude and energy dependence of R_{im} somewhat, but would not vitiate the general character of the results.

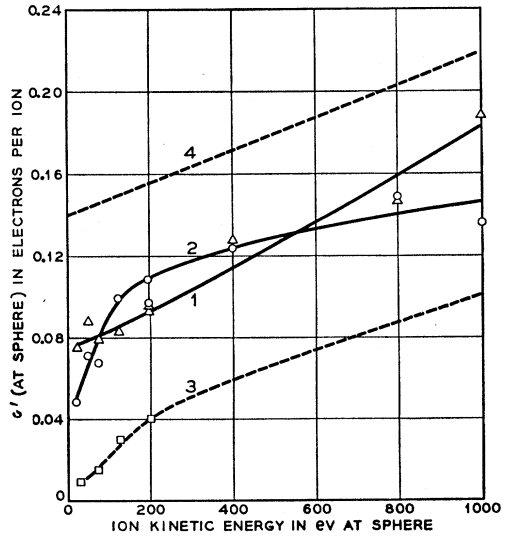

FIG. 4. γ_i' values measured for He^+, Ne^+, and Ar^+ in the clean W experiment are plotted as curves 1, 2, and 3, respectively. Curve 4 is the γ_i for He^+ on Ta measured in the work of reference 14.

TABLE II. Reflection of He^+ at clean surfaces.

$E_k(I^i)$ (ev)	Tungsten R_{ii}	Tungsten R_{im}	Molybdenum R_{ii}	Molybdenum R_{im}	Silicon (100) R_{ii}	Silicon (100) R_{im}
100	0.0017	0.0019	...	...	...	...
200	0.0018	0.0088	0.0008	0.0066	0.000024	0.00050
400	0.0015	0.020	...	...	0.000038	0.00068
600	0.0014	0.027	0.0009	0.029	0.00012	0.00075
800	0.0016	0.034	...	...	0.00015	0.0025
1000	0.0019	0.039	0.0010	0.042	0.00020	0.0030

Values of R_{ii} and R_{im} for He^+ ions on clean polycrystalline W and Mo, and the (100) face of Si are listed in Table II. Evidence for the cleanliness of these surfaces has been published elsewhere.[13,15,22,23] R_{ii} and R_{im} for He^+ on contaminated surfaces of polycrystalline W and Hf, and the (111) face of Ge are listed in Table III. These surfaces, although not clean, were not heavily contaminated either. It is possible to identify their state in terms of the Auger results published elsewhere.[17,23,24] The W surface is in the condition of curve 3 of Fig. 3 of reference 23. The Hf surface is in the cleanest condition obtained[17] which was known to be covered with at least a fraction of a monolayer. The Ge(111) surface was in the condition of curves 2 of Figs. 1 and 2 of reference 24. These contaminated surfaces are perhaps best characterized as having only tightly bound contaminants upon them.

The He^+ data for clean W from Table II are plotted in Figs. 5 and 6, in which data for Ne^+ and Ar^+ are also shown. As will be seen in the next section, we expect the phenomena governing the magnitudes of R_{ii} and R_{im} to depend on the velocity rather than the energy of the particle. Accordingly, we have investigated the velocity dependence of the data of Figs. 5 and 6. Since R_{ii} is essentially independent of energy it will also be independent of velocity. The R_{im} data of Fig. 6 are plotted on a velocity scale in Fig. 7. Here we observe

TABLE III. Reflection of He^+ at contaminated surfaces.

$E_k(I^i)$ (ev)	Tungsten R_{ii}	Tungsten R_{im}	Hafnium R_{ii}	Hafnium R_{im}	Germanium (111) R_{ii}	Germanium (111) R_{im}
100	0.00043	0.0019	0.00039	0.0023	0.0013	0.0015
200	0.00052	0.0085	0.00057	0.011	0.0025	0.023
400	0.00062	0.021	0.00075	0.045	0.0037	0.077
600	0.00084	0.032	0.00090	0.078	0.0041	0.12
800	0.0010	0.040	0.0013	0.100	0.0051	0.15
1000	0.0012	0.043	0.0016	0.121	0.0047	0.20

[22] F. G. Allen, J. Eisinger, H. D. Hagstrum, and J. T. Law, J. Appl. Phys. **30**, 1563 (1959).
[23] H. D. Hagstrum and C. D'Amico, J. Appl. Phys. **31**, 715 (1960).
[24] H. D. Hagstrum, J. Phys. Chem. Solids **14**, 33 (1960).

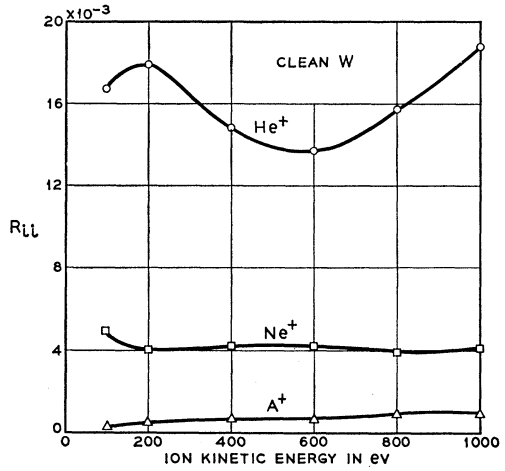

FIG. 5. R_{ii} vs ion kinetic energy for He^+, Ne^+, and Ar^+ on clean W.

the surprising result that the data now all lie approximately on the same curve.

IV. DISCUSSION

The basic experimental results of this work may be summarized as follows:

1. R_0 and its components, R_{ii} and R_{im}, are all small.
2. R_{ii} is essentially independent of ion energy whereas R_{im} increases rapidly with ion energy.
3. R_{im} has approximately the same magnitude as a function of velocity, independent of the mass or nature of the ion, for He^+, Ne^+, and Ar^+.
4. R_{ii} and R_{im} appear to have similar values for the metals whether clean or somewhat contaminated.
5. The values of R_{ii} and R_{im} for semiconductors are larger than for metals by a factor of about 5 if the surfaces are contaminated and are less by a factor of 10 if the surfaces are clean.

We suspect that these results are representative of the reflection of ions whose ionization energy is large relative to twice the work function of the solid. First, let us compare them as far as is possible with the scanty work already reported for such ions. The magnitude of R_0 is much lower than that found by Healea and co-workers[2,3] and more nearly like that found by Rostagni.[4] It should be pointed out that it is possible that the surfaces used by Healea were more heavily contaminated than any of those of the present work. Furthermore, since in this earlier work only the total electrical effects of reflection were measured with no attempt to analyze into components, the results should be compared with R_0 here and not with R_{ii} as was done by Brunnée.[11] The earlier results that reflection effects increase with ion energy are thus consistent with the increase in R_0 found here.

Bradley and co-workers[8–10] have concluded that the very slow so-called "reflected" ions (Xe^+) they see are actually sputtered from adsorbed noble gas atoms on the surface. It is difficult to see how this could be the case here, particularly for He^+. Honig[7] and Bradley and co-workers[8–10] also see positive ions of the base material. Here again, one would perhaps expect little of this for He^+ in the present work. In general, the negative ions observed to be released from surfaces[6] come from impurities adsorbed on the surface which were certainly absent in the work listed here in Table II. We also call attention to the very small ion beam intensity ($\sim 10^{-10}$ amp) used in the present work and the very small magnitudes of R_{ii} and R_{im}. All things considered, it seems reasonable that the ions and metastable atoms observed to leave the target in the present work are those of the atoms in the incident ion beam.

No detailed theory exists with which the present results may be compared. It is possible, however, to draw several conclusions and to demonstrate a consistency of the data internally and with the processes we know to be operative near the surface. We know that an ion approaching a solid surface can become involved in electronic transitions of both a resonance and an Auger type.[20] The resonance tunneling processes may, depending on the position of the excited levels in the atom relative to the Fermi level, ionize a metastable

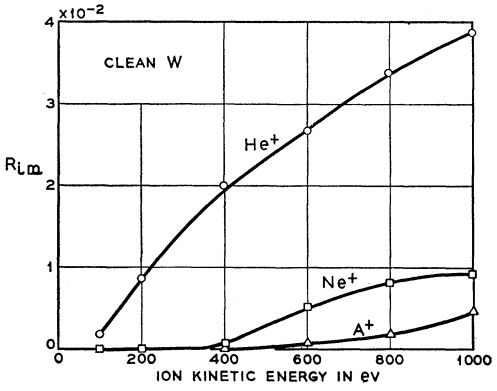

FIG 6. R_{im} vs ion kinetic energy for He^+, Ne^+, and Ar^+ on clean W.

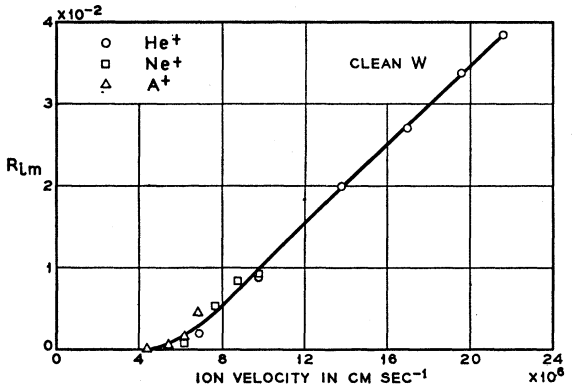

FIG. 7. R_{ii} vs ion velocity for He^+, Ne^+, and Ar^+ on clean W.

atom or neutralize an ion to an excited state. How this comes about is illustrated in Fig. 8, which is like figures already published by the author[14] and by Varnerin.[25]

Figure 8 is an energy diagram in which the potential energy of the system of atom or ion and solid is plotted as a function of the distance, s, of the atom or ion from the solid surface. In Fig. 8 the energy of the system of ion, X^+, and n electrons, e_S^- in the solid with X^+ at $s=\infty$ is taken to be zero. The system of metastable atom X^m and $(n-1)$ electrons in the solid is derived from $X^+ + ne_S^-$ by neutralizing X^+ to a metastable level with an electron drawn from the solid. Since for a metal the neutralizing electron may come from anywhere in the conduction band of width ϵ_F the levels $X^m + (n-1)e_S^-$ with X^m at $s=\infty$ will lie anywhere in a band ϵ_F wide as shown in Fig. 8. The position of this band with respect to $X^+ + ne_S^-$ at zero energy is also shown, where

$$\Delta = E_i - E_x - \varphi. \tag{10}$$

Here E_i is the ionization energy of the normal atom, E_x is the excitation energy of the metastable atom and φ is the work function of the metal. $E_i - E_x$ is thus the ionization energy of the metastable state. If $\Delta > 0$, the state of affairs shown in Fig. 8 prevails.

As the ion X^+ is brought closer to the solid surface, the state $X^+ + ne_S^-$ varies as curve 1 in Fig. 8 by virtue of the interaction between X^+ and the solid.[20] The state $X^m + (n-1)e_S^-$ varies as curve 2, there being a band of such curves lying between curves 2 and 3. By virtue of the Franck-Condon principle, resonance transitions from $X^+ + ne_S^-$ to $X^m + (n-1)e_S^-$ can occur only where curve 1 crosses some one of the curves

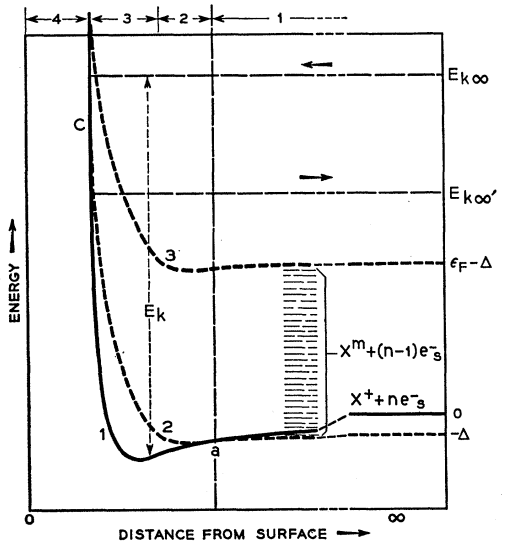

FIG. 8. Plot of energy of the systems $X^+ + ne_S^-$ and $X^m + (n-1)e_S^-$ versus distance of the atomic particle from the surface.

[25] L. J. Varnerin, Phys. Rev. **91**, 859 (1953).

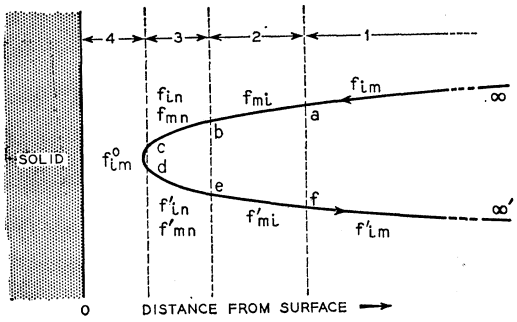

FIG. 9. Orbit of an atom near the solid surface, with indications of the fractional transformations in each of the regions defined in Fig. 8.

lying between curves 2 and 3. This occurs at distances from $s=\infty$ to the point a in Fig. 8. This has been designated region 1 at the top of the figure. At distances closer than point a the resonance process can go in the reverse direction with the ionization of X^m. The electron then tunnels into an unoccupied level in the solid above the Fermi level. This process characterizes region 2 in Fig. 8. At somewhat closer approach the Auger transitions can occur.[20] This process is Auger neutralization if the particle is an ion and Auger de-excitation if it is a metastable atom. This occurs in region 3 of Fig. 8. We designate the region of very close approach where repulsive forces are high for both ion and metastable atom and the potential curves have come very close together or, in fact, have become the same curve as region 4. We know that regions 2 and 3 overlap so that separation into distinct regions, as has been done here, is somewhat of an idealization. However, it makes further discussion easier and does not alter the basic conclusions.

In Fig. 8 we have indicated an incident ion energy toward the surface of $E_{k\infty}$. The total energy of the system is conserved at this level during the inward trip of the ion. Thus as the potential energy varies the kinetic energy varies as the length of the arrow E_k shown. It is probable that some energy of translation will be lost to the lattice in region 4 and that the kinetic energy of the particle on the outward trip will be less as indicated by the level $E_{k\infty'}$.

We have seen in Fig. 8 how three of the regions designated are to be distinguished as regards the resonance or Auger processes which can occur in each. A fourth region of close approach to the solid is also designated. These are shown again schematically in Fig. 9 together with an orbit of approach of an atom to and recession from the surface. The f factors indicated in each region are the fractions of particles entering the region which undergo the transformation indicated in the subscripts. Thus, in region 1 a fraction f_{im} of ions are transformed on the inward trip from ions, i, to metastable atoms, m, and a fraction f_{im}' undergo the same transformation on the outward trip. Similar definitions hold for regions 2 and 3. In region 3

TABLE IV. Expressions for the ratios N_m^x/N_i^∞ and N_i^x/N_i^∞.

x	N_m^x/N_i^∞ (a) $f_{im}, f_{im}' \neq 0$	N_m^x/N_i^∞ (b) $f_{im}=f_{im}'=0$	N_i^x/N_i^∞ (a) $f_{im}, f_{im}' \neq 0$	N_i^x/N_i^∞ (b) $f_{im}=f_{im}'=0$
∞	0	0	1	1
a	f_{im}	0	$1-f_{im}$	1
b	$f_{im}(1-f_{mi})$	0	$1-f_{im}+f_{im}f_{mi}$	1
c	$f_{im}(1-f_{mi})(1-f_{mn})=A$	0	$(1-f_{im}+f_{im}f_{mi})(1-f_{in})=B$	$1-f_{in}$
d	$A+Bf_{im}^0$	$(1-f_{in})f_{im}^0$	$B(1-f_{im}^0)$	$(1-f_{in})(1-f_{im}^0)$
e	$(A+Bf_{im}^0)(1-f_{mn}')=C$	$(1-f_{in})f_{im}^0(1-f_{mn}')=D$	$B(1-f_{im}^0)(1-f_{in}')=E$	$(1-f_{in})(1-f_{im}^0)(1-f_{in}')=F$
f	$C(1-f_{mi}')$	$D(1-f_{mi}')$	$E+Cf_{mi}'$	$F+Df_{mi}'$
∞'	$C(1-f_{mi}')+(E+Cf_{mi}')f_{im}'$	$D(1-f_{mi}')$	$(E+Cf_{mi}')(1-f_{im}')$	$F+Df_{mi}'$

ions are transformed to neutral atoms, n, in the ground state via Auger neutralization and metastable atoms to ground-state atoms via Auger de-excitation. The symbol f_{im}^0 in region 4 indicates that ions are changed to metastable atoms very close to the surface, which process will be discussed shortly.

It is now possible to write down expressions for the relative number of ions and metastable atoms at each of the division points between the numbered regions of Fig. 9 on both inward and outward trips. We use the symbols N_m^x and N_i^x to indicate the number of metastable atoms and ions, respectively, at position x. x may be ∞, a, b, c, d, e, f, or ∞' (Fig. 9). In Table IV may be found expressions for the ratios N_m^x/N_i^∞ and N_i^x/N_i^∞ determined for the two cases: (a) $f_{im}, f_{im}' \neq 0$, and (b) $f_{im}=f_{im}'=0$.

We point out first of all that all four of the regions shown in Figs. 8 and 9 for the general case may not exist for any particular ion and surface. The point a may lie at $s=\infty$ and region 1 thus not exist if $\Delta \leq 0$ [Eq. (10)], as is true for Ar^+, Kr^+, and Xe^+ incident on tungsten.[20] Or region 1 will not exist if point a lies at such large s that wave function overlap is so small as to make the resonance probability and hence f_{im} and f_{im}' essentially zero. This latter is the case for He^+ on W.[20] Thus for He^+, Ar^+, Kr^+, and Xe^+ case (b) ($f_{im}=f_{im}'=0$) applies. This is fortunate since case (a) leads to quite complicated expressions as is seen in Table IV.

We now show that the present experimental results cannot be accounted for by the processes of regions 1, 2, and 3 alone for f_{im} and f_{im}' either zero or finite. First, if $f_{im}=f_{im}'=0$ we see that in regions 1, 2, and 3 there is no mechanism of transforming ions to metastable atoms as is required by the experimental results (item 2 of summary above). If f_{im} and f_{im}' are not zero, a mechanism of changing ions to metastable atoms then exists but it has the wrong dependence on ion energy. As ion energy is increased it is reasonable to assume that the time spent in region 1 decreases on both the inward and outward trips and that, as a consequence, both f_{im} and f_{im}' decrease. However, the experimental results show that the number of reflected metastable atoms increases with ion energy. Thus, in either case, another mechanism of transforming ions to metastable atoms is needed. The only likely place is in the region of closest approach, region 4, where the fraction changed from ions to metastable atoms is indicated as f_{im}^0.

It is suggested that a reasonable mechanism to account for the factor f_{im}^0 in region 4 is the following. In this region repulsive energies are high and the potential curves of Fig. 8 for ion and metastable atom are close together, if not coincident. In fact, in this region it is perhaps impossible or meaningless to distinguish ion and metastable atom from one another since the electronic structure of the atom overlaps that of the solid so strongly. Should the nucleus separate itself from the solid, there will be a definite probability that the electronic structure of the separated atom will be that of the ion (curve 1) or that of the metastable atom (one of the curves between curves 2 and 3). This probability should be independent of the nature of the particle as between ion and metastable atom and its velocity as it enters region 4. What this means is that conditions in region 4 are such as to re-establish the possibility of ready electron transfer between the metastable level in the atom and the solid. Thus, region 4 is thought to be analogous to the "störgebeit" postulated by Weizel and Beeck[26] to occur on close approach of an ion and neutral gas atom and used by them to account for ionization and excitation of free atoms by ion impact. This assumption is equivalent to saying that at point d on the outward trip there is a definite ratio of the number of positive ions (N_i^d) to the number of metastable atoms (N_m^d):

$$N_m^d = kN_i^d. \tag{11}$$

For case (b) it can be shown from Table IV that

$$k = f_{im}^0(1-f_{im}^0). \tag{12}$$

Thus it is consistent to take k and f_{im}^0 as constants characteristic of the ion and surface in question.

In terms of the expressions of Table IV, case (b) we

[26] W. Weizel and O. Beeck, Z. Physik **76**, 250 (1932).

may now write:

$$R_{ii}=N_i^{\infty\prime}/N_i^{\infty}=(1-f_{in})(1-f_{im}^{0})(1-f_{in}')+(1-f_{in})f_{im}^{0}(1-f_{mn}')f_{mi}', \quad (13)$$

and

$$R_{im}=N_m^{\infty\prime}/N_i^{\infty}=(1-f_{in})f_{im}^{0}(1-f_{mn}')(1-f_{mi}'). \quad (14)$$

We shall now use these expressions in a discussion of the five basic experimental results listed above.

R_{ii} and R_{im}, and hence R_0, are small (item 1) because of the high Auger probabilities. This means that f_{in} and f_{mn} are large, $(1-f_{in})$ and $(1-f_{mn})$ small, in expressions (13) and (14) making both R_{ii} and R_{im} small.

We may make a consistency argument concerning the energy or velocity dependence of R_{ii} and R_{im} (item 2) using expressions (13) and (14) as follows. We assume that as incident ion velocity increases, velocity on the outward trip also increases. Thus, the particle spends less time in any given region and the f factor decreases, $(1-f)$ increases with increasing ion velocity. Taking expression (14) for R_{im} first, we see that except for the constant factor f_{im}^{0} all other f factors enter as $(1-f)$ so the total expression must increase in magnitude as incident ion velocity increases in agreement with experiment. In expression (13) for R_{ii}, f_{mi}' appears alone in the second term giving rise to the possibility that this term could decrease if the effect of decrease in f_{mi}' outweighs the increase in the terms $(1-f_{in})$ and $(1-f_{mn}')$. Thus, the whole second term in (13) could decrease and tend to compensate the first term which can only increase. This possibility is at least consistent with the experimental observation that R_{ii} is approximately independent of ion velocity.

The third experimental result (item 3 and Fig. 7) is the surprising one that R_{im} for He^+, Ne^+, and Ar^+ has approximately the same value at the same incident ion velocity. This must require that the various f factors for these ions in expression (14) are either (a) all very nearly the same in magnitude, or (b) have such magnitudes as to make the over-all expression nearly the same for these ions. This is the more surprising because R_{im} depends not on f_{in} and f_{mn}', but $(1-f_{in})$ and $(1-f_{mn}')$ which are small.

There appear to be no reasons which can be given for the relative behavior of the metals among themselves or as compared to the semiconductors (items 4 and 5).

ACKNOWLEDGMENT

It is a pleasure to acknowledge the assistance of C. D'Amico in obtaining the experimental data on which the present work is based.